CI

e-med
www.e-med.org.uk

ORIGINAL ARTICLE

Imaging features of primary anorectal gastrointestinal stromal tumors with clinical and pathologic correlation

M.R. Koch[a], J.P. Jagannathan[a,b], A.B. Shinagare[b], K.M. Krajewski[b], C.P. Raut[c], J.L. Hornick[d], N.H. Ramaiya[b]

[a]*Department of Radiology, Brigham and Women's Hospital, 75 Francis Street, Boston, MA 02115, USA;* [b]*Department of Imaging, Dana-Farber Cancer Institute, 450 Brookline Avenue, Boston, MA 02115, USA;* [c]*Department of Surgery, Brigham and Women's Hospital, 75 Francis Street, Boston, MA 02115, USA;* [d]*Department of Pathology, Brigham and Women's Hospital, Boston, MA, 02115, USA*

Corresponding address: Atul B. Shinagare, MD, Department of Imaging, Dana-Farber Cancer Institute, 450 Brookline Avenue, Boston, MA 02115, USA.
Email: `ashinagare@partners.org`

Abstract

Purpose: To evaluate the imaging features of anorectal gastrointestinal stromal tumors (GISTs) with clinical and histopathologic correlation. **Materials and methods:** In this Institutional Review Board-approved, Health Insurance Portability and Accountability Act-compliant retrospective study, 16 patients (12 men; mean age 66 years (30–89 years)) with pathologically proven anorectal GISTs seen at our institution from January 2001 to July 2011 were identified. Electronic medical records were reviewed to obtain clinical data. Pretreatment imaging studies (computed tomography (CT) in 16 patients, magnetic resonance imaging (MRI) in 9 patients and fluorodeoxyglucose (FDG)-positron emission tomography (PET)/CT in 8 patients) were evaluated by 2 radiologists until consensus. The location, size and imaging features of the primary tumor and metastases at presentation, if any, were recorded, and correlated with clinical data and pathologic features (histologic type, presence of necrosis, mitotic activity, risk category, immunohistochemical profile). **Results:** The mean tumor size was 6.9×6.0 cm. Of the 16 tumors, 11 (68.7%) were infralevator, 4 (25%) supra and infralevator and 1 (6.3%) supralevator; 9 (56.2%) were exophytic, 6 (37.5%) both exophytic and intraluminal, and 1 (6.3%) was intraluminal. The tumors were iso- to minimally hypoattenuating to muscle on CT, iso- to minimally hypointense on T1-weighted images, hyperintense on T2-weighted images and showed variable enhancement. Necrosis was seen in 4 (25%), and hemorrhage and calcification in 2 (12.5%) patients each. The tumors were FDG avid with a mean maximum standardized uptake value of 11 (8.4–16.8). All tumors were positive for KIT and CD34. Distant metastasis to liver was seen in 1 patient (6.3%) at presentation. **Conclusion:** Anorectal GISTs are well-circumscribed, non-circumferential, predominantly infralevator, intramural or exophytic, FDG-avid, hypoattenuating masses, and present without lymphadenopathy or intestinal obstruction.

Keywords: *Gastrointestinal stromal tumor; anorectal; CT; MRI; FDG-PET/CT.*

Introduction

Gastrointestinal stromal tumors (GISTs) are the most common clinically significant mesenchymal neoplasms of the gastrointestinal tract, most frequently arising in the stomach (60–70%) or small bowel (20–30%)[1]. Anorectal GISTs are rare, accounting for 5% of all GISTs and only 0.1% of all anorectal tumors[2]. The clinicopathologic features of anorectal GISTs are most similar to GISTs arising in the small bowel. Although the exact cell of origin of GISTs is unclear, GISTs are believed to arise from the pacemaker cell of the gut, the interstitial cells of Cajal or from a common mesenchymal precursor cell[3]. Approximately 80–85% of GISTs harbor activating mutations of the *KIT* tyrosine kinase gene[4]. KIT immunoreactivity is useful for distinguishing GISTs from other mesenchymal neoplasms, and the mutant constitutively active KIT protein serves as a

target for therapy[5]. There has been increased interest in this uncommon entity after the introduction of the tyrosine kinase inhibitor, imatinib mesylate (Gleevec®, Novartis, Switzerland), which has revolutionized the treatment of GISTs and is considered the prototype of the emerging science of molecular-targeted therapy[6].

Most of the published literature on anorectal GISTs has focused on the pathology and clinical behavior, and the literature on imaging features of anorectal GISTs is limited to a few case reports and small cases series[7–10]. The purpose of this study was to review the appearance of anorectal GISTs on magnetic resonance imaging (MRI), computed tomography (CT) and positron emission tomography (PET), and highlight the distinguishing imaging features that help to differentiate these tumors from the more common rectal tumors.

Materials and methods

Subjects

In this Institutional Review Board-approved, Health Insurance Portability and Accountability Act-compliant retrospective study, informed consent was waived. Sixteen patients (12 men, 4 women; mean age 66 years (range 30–89 years, median 68 years)) with pathologically proven anorectal GISTs who were seen at our institution between January 2001 and July 2011 were identified from a pathology registry through a query for patients with a diagnosis of rectal GIST on biopsy or surgical resection. The electronic medical records were retrospectively reviewed for clinical information including age, gender, presenting symptoms, clinical management and outcome.

Imaging

A systematic review of all available imaging studies, including CT, MRI and PET/CT was performed with consensus by 2 radiologists with expertise in cancer imaging (N.R. and J.J.), with 11 and 10 years of experience, respectively. At presentation, all 16 patients had CT studies, 9 patients underwent MRI and 8 patients underwent fluorodeoxyglucose (FDG)-PET/CT. A contrast-enhanced CT scan of the abdomen and pelvis was available in all 16 patients. MRI was performed using an endorectal coil in 6 patients and a body coil in 3 patients. Six patients underwent MRI with intravenous gadolinium contrast. Three patients underwent MRI without contrast. All patients had T1-weighted and fast spin-echo T2-weighted images. Because the study design was retrospective and patients were referred to our tertiary cancer center from several institutions with imaging already performed on a variety of equipment and differing protocols, there was considerable variation in the imaging technique.

The imaging protocol for a newly diagnosed anorectal mass at our institution includes rectal MRI for local staging, and contrast-enhanced CT scan of the chest, abdomen and pelvis for assessment of metastatic disease. FDG-PET/CT is not routinely performed as part of the initial staging workup. The protocols and techniques at our institution are as follows.

CT protocol

CT scans of the abdomen/pelvis and/or chest are performed on 64-row multidetector CT (MDCT) scanner (Aquilion 64; Toshiba America Medical Systems, Irvine, CA) with the following parameters: (1) 64-row MDCT scanner at 0.5 mm collimation, 120 kVp, tube current maximum of 500 mA using dose modulation with a noise index of 12.5 HU, 0.5 s gantry rotation time, and a table speed of 26.5 mm per rotation. One hundred milliliters of iopromide (300 mg I/ml; Ultravist 300; Bayer HealthCare Pharmaceuticals, San Francisco, CA) are injected intravenously with an automated injector (Stellant; Medrad, Warrendale, PA) at a rate of 2–3 ml/s, with a scan delay of 60 s. 750–1000 ml of a 3% solution of diatrizoate meglumine and sodium (Gastrografin; Bracco Diagnostics, Princeton, NJ) are administrated prior to all CT scans. Axial images with 5-mm thickness and coronal images with 4-mm thickness are reconstructed using standard abdomen algorithms, transferred to the picture-archiving communication system and subsequently reviewed on a commercial workstation (Centricity, General Electric, Barrington, IL).

MRI protocol

Imaging is performed on either a 1.5-T MR system (Signa HDx; GE Medical Systems, Milwaukee, WI) or a 3-T MR system,(Siemens Trio Tim; Siemens Healthcare, Erlangen, Germany) using a phased array body coil. We do not routinely use endorectal coil MRI due to difficulty in coil placement and limited field of view (FOV), which poses problems with bulky tumors. Our MRI protocol for evaluation of anorectal tumors consists of sagittal T2-weighted single-shot images (for tumor localization), axial and coronal T2-weighted fast spin-echo (FSE) images. Small FOV (16–32 cm) high-resolution oblique axial images are obtained with a slice thickness of 3 mm, perpendicular and parallel to the tumor axis. Unenhanced and contrast-enhanced fat-suppressed three-dimensional T1 axial images and post-contrast sagittal and coronal T1-weighted images are also obtained. Coronal T2 FSE images are especially helpful in assessing the relationship of low rectal tumors to levator ani and the anal sphincters. Images are transferred to the picture-archiving communication system and subsequently reviewed on a workstation (Centricity, General Electric, Barrington, IL).

[18F]FDG-PET/CT protocol

FDG-PET imaging is performed according to the standard clinical protocol. Patients are instructed to minimize

vigorous physical activity for 24 h before the scans and follow a minimum 6-h fast before the injection of FDG. Approximately 15–20 mCi of [^{18}F]FDG is administered intravenously. PET imaging from the skull base to mid-thigh is performed approximately 60 min after the FDG injection. The patients are scanned on a dedicated PET/CT scanner (GE Discovery ST 16, Milwaukee, WI or Siemens Biograph 16, Knoxville, TN). All PET images are reconstructed with iterative methods (OSEM), and corrected for attenuation, detector efficiency, scatter, decay, dead time, and random coincidences. The PET and CT images are accurately co-registered on dedicated a workstation using syngo software (Siemens Medical Solutions, Erlangen, Germany). PET and CT datasets are viewed separately as well as in fused mode.

Image analysis

Image analysis for CT and MRI was performed on a dedicated workstation (Centricity, General Electric, Barrington, IL), and PET/CT images were reviewed on a Siemens workstation using syngo software, Syngo MMWP Version 31A (Siemens Medical solutions, Erlangen, Germany). On CT, the location, maximal size, contour, margin, attenuation, and enhancement pattern were recorded. The attenuation of the mass was measured using a region of interest drawn manually to encompass the entire tumor on the axial images, while being careful not to include surrounding tissue. The location was defined in 2 planes. In the coronal plane, the location was divided into 3 categories, namely supralevator, supra- and infralevator, and infralevator, based on the relationship of the tumor with the levator ani muscle. Coronal MRI images were used for this purpose in the 9 patients who underwent MRI. For the 7 patients who did not undergo MRI, coronal CT images were used. If coronal CT images were not available, the coronal images were reconstructed using multiplanar reformatting on a commercially available workstation (Vitrea 4.1, Vital Images, Inc). On the axial plane, the position of the tumor was described along the circumference of the rectal wall, as anterior, anterolateral, lateral, posterolateral and posterior. The supralevator space and ischiorectal fossa were evaluated for extension of the tumor. The presence or absence of hemorrhage, necrosis or calcification within the tumor, and secondary CT findings such as lymphadenopathy, the presence of bowel obstruction and distant metastasis were also documented. Lymphadenopathy was defined by standard criteria for lymph nodes with a short axis greater than 1 cm for pelvic and retroperitoneal locations, and greater than 1.5 cm for inguinal locations.

On MRI, the primary sequences used for assessment were the FSE T2-weighted images (for size, contour, margin, and signal intensity) and the axial post-contrast T1-weighted images for enhancement characteristics. Enhancement was categorized as mild, moderate or avid in comparison with the enhancement of the adjacent muscles. Diffusion-weighted images were not obtained routinely, and were not included in the analysis. In addition, the relationship of the tumor to the levator ani insertion was recorded on the coronal FSE T2-weighted images. Mucosal involvement was assessed on MRI on T2-weighted images, and was considered to be present if there was focal discontinuity of the innermost layer of the rectum overlying the tumor, with or without irregularity.

PET/CT images were analyzed by 2 radiologists with consensus. The FDG-PET/CT studies were evaluated for regions of increased tracer uptake and maximum standardized uptake values (SUV$_{max}$) were calculated for uptake quantification by drawing a region of interest and, using vendor-specific software, the degree of FDG avidity and the SUV$_{max}$ were recorded.

Pathology

Pathology records from biopsy and surgical specimens from each patient were reviewed to record the following: tumor type (spindle cell, epithelioid or mixed), mitotic count, presence or absence of necrosis, and results of immunohistochemical studies, which were confirmed by an experienced pathologist (J.L.H.) with expertise in GISTs. Mitotic rate was recorded as the number of mitoses per 50 high-power fields (HPF) or as the number of mitoses per 10 HPF when only small tissue samples were available. Based on tumor size and mitotic index, using previously published criteria, risk stratification of the tumors was performed[11–13]. Immunohistochemistry for KIT was performed in all cases. Other markers, including CD34, SMA, S-100, desmin, DOG1, and caldesmon, were performed in some cases. Correlation between the imaging and histopathologic findings was made by consensus between the radiologist (J.J) and the pathologist (J.L.H).

Results

Clinical findings

The study population consisted of 12 men and 4 women, with a mean age of 66 years (range 30–89 years, median 68 years). The mean age for the 4 women was 73 years (range 68–84 years) and the mean age for the 12 men was 63 years (range 30–89 years). Eight patients were asymptomatic, the rectal mass being found on routine rectal or gynecologic examination in 7 patients, and on CT performed after a motor vehicle accident in 1 patient. Among the 8 symptomatic patients, 3 patients presented with rectal bleeding and pain, 2 presented with perirectal discomfort, 1 with constipation and rectal bleeding, 1 with constipation and rectal fullness, and 1 with acute abdominal pain was initially misdiagnosed as prostatic abscess and drained before pathology revealed a GIST.

Surgical resection was performed in 14/16 patients. Before surgery, 11/14 patients underwent neoadjuvant

Table 1   **Morphology and pathologic characteristics of anorectal GISTs**

Patient no.	Location	Circumferential location	Growth pattern	Maximum dimension (cm)	Mitotic count (HPF)	Risk
1	Infralevator	Lateral	Exophytic/intraluminal	4.3	<1/10	Low
2	Infralevator	Anterior	Exophytic	7	21/50	High
3	Supralevator	Anterolateral	Exophytic/intraluminal	11	21/50	High
4	Infralevator	Posterolateral	Exophytic/intraluminal	6.3	8/10	High
5	Supra and infralevator	Anterior	Exophytic	10.2	<1/10	High
6	Supra and infralevator	Anterolateral	Exophytic	11.3	13/50	High
7	Supra and infralevator	Anterolateral	Exophytic	6.3	15/10	High
8	Infralevator	Anterior	Exophytic/intraluminal	7	7/50	High
9	Infralevator	Posterolateral	Exophytic	2	18/50	High
10	Infralevator	Anterior	Exophytic/intraluminal	6.6	7/50	High
11	Infralevator	Anterior	Exophytic	8.4	9/50	High
12	Infralevator	Posterior	Exophytic/intraluminal	7	2/10	High
13	Infralevator	Posterior	Intraluminal	1.7	2/50	None
14	Infralevator	Posterolateral	Exophytic	5.8	<1/10	Moderate
15	Supra and infralevator	Anterolateral	Exophytic	6.6	N/A	N/A
16	Infralevator	Anterolateral	Exophytic	9.1	13/10	High

chemotherapy with imatinib mesylate (Gleevec) for a mean time interval of 307 (75–510 days). Surgery was not performed on 2 patients (1 patient with metastatic disease to the liver and in the second patient surgery was deferred due to multiple co-morbidities), and at the time of completion of study, they remain on palliative imatinib therapy. The mean time interval between the last imaging study and surgical resection was 32 days (range 1–85 days). 6/14 (43%) underwent low anterior resection, and 4/14 (29%) had transanal excision, and 2/14 (14%) had abdominoperineal resection. Transphincteric sleeve resection was performed in 1 patients and transcoccygeal resection was performed in one patient.

Imaging findings

Important morphologic features of the tumors included in this study are summarized in Table 1. Eleven of 16 (68.7%) tumors were infralevator (Fig. 1), 4/16 (25%) were both supra- and infralevator (Fig. 2), and 1/16 (6.3%) tumor was completely supralevator. Two of the infralevator tumors were very low lying, close to the anal verge. The mean distance of the infralevator tumors from the anal verge was 2.9 cm (range 0.8–4 cm). All the tumors were well circumscribed, and 7 tumors were round with smooth margins, 6 were lobulated, 2 were dumbbell shaped and 1 was ovoid. None of the tumors had irregular or infiltrative margins. The mean tumor size was 6.9×6.0 cm, ranging in size from 1.7 to 11.3 cm in the long dimension and 0.6 to 10 cm in the short dimension. Seven out of 8 incidentally detected tumors in our series were more than 5 cm in size (range 5.8–11.3 cm). There was good correlation between tumor size measured on CT and MRI. A purely exophytic growth pattern was seen in 9/16 (56.2%); both exophytic and intraluminal components were present in 6/16 (37.5%), and in 1/16 (6.3%) tumors were predominantly intraluminal.

Figure 1 **A 30-year-old man with an anorectal GIST. Coronal T12-weighted MR image shows a small well-defined T2 hyperintense infralevator intersphincteric mass (arrow).**

Table 1 gives the location of tumors with respect to the levator ani muscle on coronal images, and the location along the rectal circumference in the transverse plane. Ten of 16 (62.5%) tumors were located anteriorly or anterolaterally, and contacted the prostate causing a mass effect. Invasion into the prostate was suspected on CT in 2 (12.5%) patients, however at surgery, the masses were free from the prostate. In 2 other patients where the CT suggested invasion/mass arising from the prostate, MRI performed subsequently showed a clear fat plane between the mass and the prostate.

On CT, 12/16 (75%) tumors were intermediate in attenuation and isodense to the muscle. One tumor was very low in attenuation and initially thought to be an intersphincteric cyst. Most of the tumors showed mild
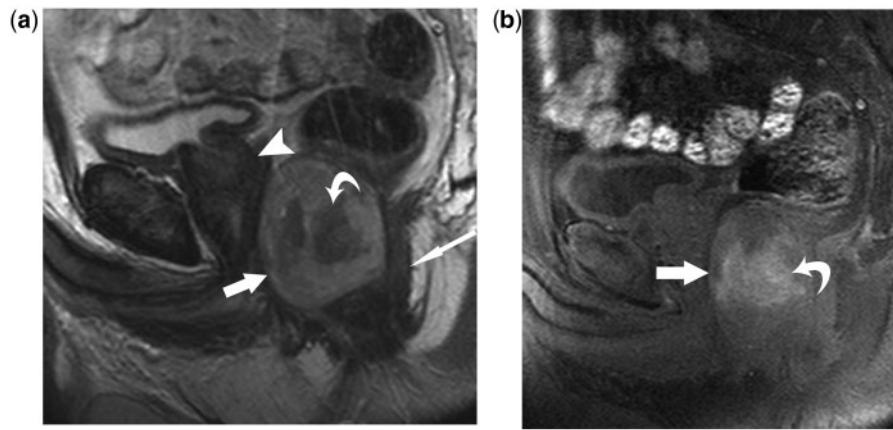
Figure 2 **A 63-year-old man with rectal GIST. (a) Sagittal T2-weighted MR image shows an exophytic predominantly hyperintense supra- and intralevator mass (arrow) with central low intensity areas (curved arrow) closely associated with and displacing the rectum (long thin arrow). The mass closely abuts the prostate (arrowhead) without evidence of invasion. (b) Sagittal T1-weighted MR image shows hyperintense areas within the mass (arrow) suggestive of intratu-moral hemorrhage. A central T1-hyperintense area is noted suggestive of hemorrhage (curved arrow).**

Table 2 **CT and MRI features of anorectal GISTs**

Patient no.	CT	T1	T2	Heterogeneity	Enhancement	Necrosis	Calcification	Hemorrhage	SUV$_{max}$
1	Iso	Hypo	Hyper	Homogeneous	Mild	N	N	N	N/A
2	Hypo	N/A	N/A	Homogeneous	Moderate	N	N	N	N/A
3	Cystic mass with foci of air	Hypo with hyper areas	Hyper	Heterogeneous	Rim enhancement[a]	Y	N	Y	N/A
4	Iso	N/A	N/A	Homogeneous	Mild	N	N	N	8.4
5	Iso	N/A	N/A	Heterogeneous	Mild	Y	Y	N	N/A
6	Iso	N/A	N/A	Heterogeneous	Moderate	N	N	N	10.9
7	Iso	Iso	Hyper	Heterogeneous	Moderate	N	N	N	9.4
8	Iso	Iso	Hyper	Heterogeneous	Moderate	N	N	N	8.7
9	Iso	N/A	N/A	Homogeneous	Moderate	N	N	N	N/A
10	Hypo	N/A	N/A	Heterogeneous	Moderate	N	N	N	11.2
11	Iso	Iso	Hyper	Homogeneous	Moderate	N	Y	N	16.8
12	Iso	N/A	N/A	Heterogeneous	Mild	N	N	N	13.1
13	Hypo	Hypo	Hyper	Homogeneous	Avid	N	N	N	N/A
14	Iso	Iso	Hyper	Heterogeneous	Moderate	Y	N	N	N/A
15	Iso	Iso with hyper areas	Hyper with hypo areas	Heterogeneous	Moderate	Y	N	Y	N/A
16	Iso	Iso	Hyper	Heterogeneous	Moderate	N	N	N	9.2

Iso, isodense/isointense; Hypo, hypodense/hypointense; Hyper, hyperintense; N/A, not available.
[a]Necrotic mass with foci of air, thought to be an abscess.

to moderate heterogeneous enhancement with focal areas of low attenuation. Central amorphous calcification was seen in 2 tumors.

On MRI, most tumors were iso- to minimally hypointense to muscle on T1-weighted images and hyperintense on T2-weighted images. The presence of hemorrhage, seen as high signal intensity foci on the fat-suppressed T1-weighted images, was seen in 2 tumors. Post-gadolinium MRI images showed mild to moderate enhancement in all but 1 patient who showed avid enhancement (Table 2). The enhancement pattern was similar on CT and MRI. One anal tumor was very low in attenuation and thought to be an intersphincteric cyst (Fig. 1). In 1 patient, the tumor presented on CT as a large rim-enhancing mass with central low density and foci of air, and was initially thought to be a prostatic abscess. Percutaneous catheter drainage was attempted, returning only minimal blood-stained fluid. Subsequent endorectal MRI showed a large necrotic pelvis mass separate from the prostate displacing the rectum (Fig. 3). At surgery, there was extensive ulceration of the rectal mucosa, and the foci of air was thought to be secondary to fistulous communication with the rectum.
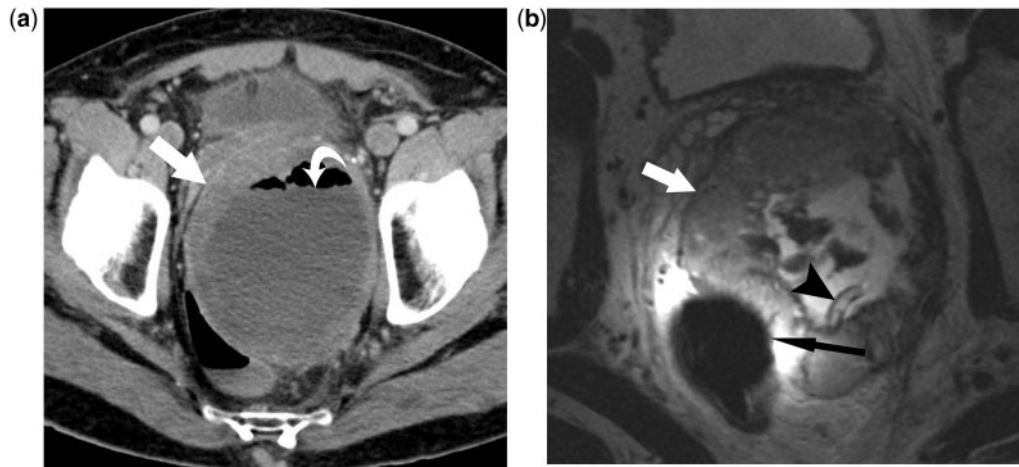
Figure 3 A 68-year-old man presented with acute severe pelvic pain. (a) Contrast-enhanced CT image in the axial plane showed a large cystic mass (arrow) with an air-fluid level (curved arrow), which was interpreted as a pelvic abscess and was drained. Pathology revealed a GIST. (b) T2-weighted MRI performed with an endorectal coil in the axial plane shows a large cystic mass with a peripheral rind of soft tissue (arrow) with central debris. A drainage catheter is seen in situ (arrowhead). Evaluation of a portion of the tumor abutting the endorectal coil is limited due to artifacts of the coil (long thin arrow).

Mucosal involvement was seen on MR images in 4/16 (25%) of patients, and was confirmed on endoscopy in 3 cases. Expansile growth with extension into the perirectal fat and ischiorectal fossa was present in 4/16 (25%) cases. Perirectal, pelvic, or retroperitoneal adenopathy was not present in any patient. Distant metastases to the liver were present in 1 patient (6.3%) at presentation.

Of the 8 patients who underwent pretreatment FDG-PET/CT, all of the tumors demonstrated moderate to intense FDG uptake (Fig. 4). Maximal standardized uptake values (SUV_{max}) ranged from 8.4 to 16.8, with a mean value of 11. In 1 patient, in addition to the FDG-avid primary rectal mass (SUV_{max} 9.2), an FDG-avid lesion with an SUV_{max} of 8.4 was seen in the left lobe of the liver, which was pathologically proved to be a metastasis.

Pathology

Histologically, 15/16 (93.7%) tumors were of spindle cell type (Fig. 5) and 1/16 (6.3%) was of mixed histology, predominantly epithelioid type. Immunohistochemical (IHC) studies were performed in all cases; 16/16 (100%) tumors were positive for KIT (Fig. 5). All tumors ($n = 10$) tested for CD34 were also positive (100%). IHC for desmin ($n = 10$) was negative in all cases (100%). In 9 cases, IHC was performed for S-100 and was negative in 7 cases (78%) and positive in 2 cases (22%). SMA was negative in 7 of 9 tumors tested (78%) and positive in 2 (22%). Mitotic rate ranged from 1 to 21 per 50 HPF. Based on tumor size (documented on initial imaging) and mitotic rates, 1/16 (6.3%) tumor was classified as having no risk for malignant behavior, 1 (6.3%)
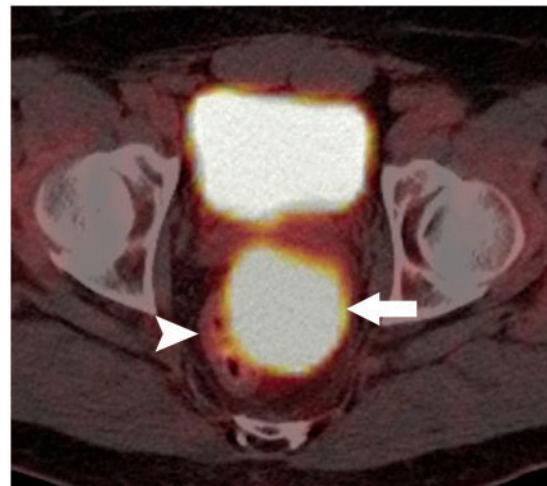

Figure 4 A 62-year-old man with rectal GIST. Fused FDG-PET/CT image in the axial plane shows a large intensely FDG-avid mass (arrow) closely abutting and displacing the rectum (arrowhead). Physiologic FDG activity is seen in the urinary bladder.

was considered low risk, 1 (6.3%) with moderate risk, and 12/16 (75%) were considered high risk (Table 1). Risk stratification could not be performed on 1 (6.3%) tumor, as the mitotic rate could not be accurately assessed on the small pretreatment biopsy. Necrosis was present on the biopsy specimens in 4/16 (25%) tumors, all of which belonged to the high-risk category. Two tumors were analyzed for the presence of *KIT* gene mutations; a typical *KIT* exon 11 mutation was detected in both cases.
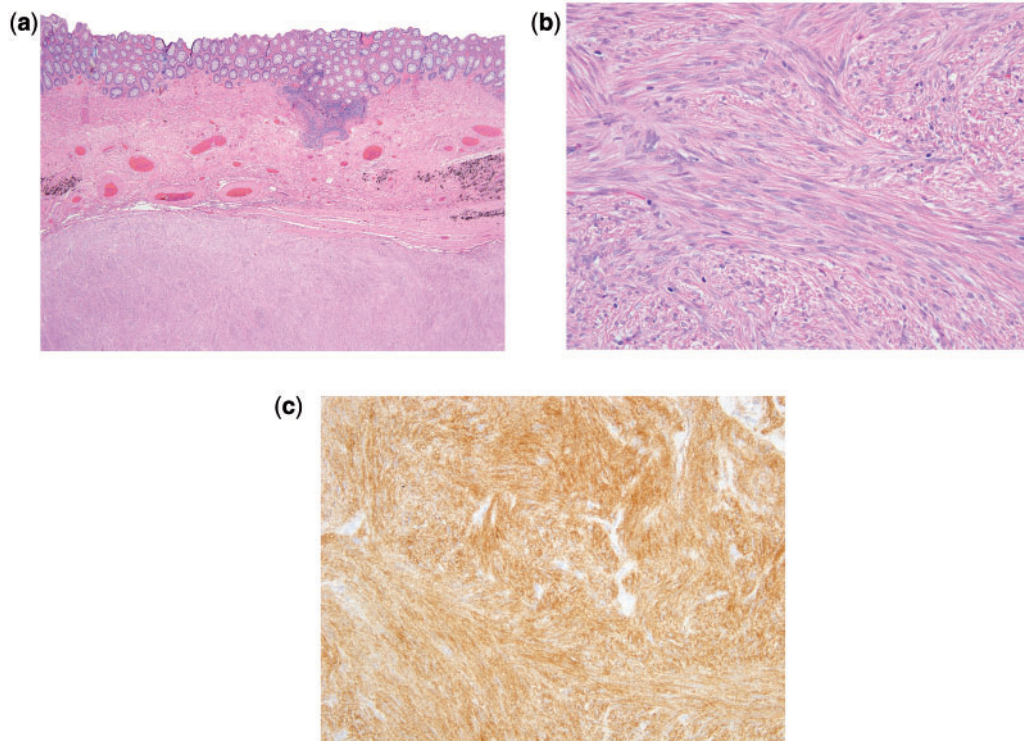
Figure 5 **(a) Low-power image stained with hematoxylin and eosin of a rectal GIST showing the tumor located in the muscularis propria. (b) High-power image stained with hematoxylin and eosin shows that the tumor is composed of fascicles of uniform spindle cells with elongated nuclei and palely eosinophilic cytoplasm. (c) Immunohistochemistry image showing diffuse positivity for KIT. The tumor also showed diffuse positivity for CD34 (not shown).**

Discussion

To our knowledge, this is the largest report on multimodality imaging features of anorectal GISTs. Although GISTs are the most common malignant mesenchymal neoplasms of the gastrointestinal tract, anorectal GISTs are rare. GISTs are thought to derive from the interstitial cells of Cajal or a precursor cell[3,4], which in the rectum form a network surrounding the autonomic nerves of the Auerbach (myenteric) plexus and are distributed within the inner and outer layer of the muscularis propria[14]. GISTs typically arise in the bowel wall and exhibit an expansile growth pattern. Clinical and pathologic studies on anorectal GISTs have been published, but the literature on the imaging findings is limited to case reports and small cases series.

In our study, anorectal GISTs showed a distinct predilection for older age, mean age of 66 years (range 30–89 years) and male predominance (3:1), consistent with several other series[15,16]. In half of the cases, the tumor was found incidentally, contrary to several previous series, where anorectal GISTs, especially when large, were most commonly symptomatic, often presenting with rectal bleeding[15,17,18]. Most of the tumors detected incidentally in our series were larger than 5 cm. Among the symptomatic patients, rectal pain (31%) and bleeding

(25%) were the most common symptoms. None of the patients presented with bowel obstruction.

GISTs have been reported to occur along the entire length of the rectum all the way to the pectinate line and anus[15]. In our study, most (68.7%) of the tumors were located below the levator ani muscle. All but 1 patient had either exophytic (56.2%) or exophytic and intraluminal (37.5%) tumors, and 62.5% tumors were located anteriorly or anterolaterally. The tumors located along the anterior rectal wall may abut the prostate, however, prostatic invasion was not found at surgery in any of our patients. On CT, although prostatic invasion was suspected in 4 patients due to similar intermediate attenuation of the tumor and the prostate, in 2 patients subsequent MRI demonstrated a clear fat plane between the mass and the prostate, and in the other 2 patients the mass was free from the prostate at surgery.

The greatest dimension of the tumor varied in size from 1.7 to 11 cm with a mean largest tumor dimension of 6.9 cm. There was good correlation between the maximum tumor size measured on CT and MRI. On CT, the tumors were predominantly iso- to minimally hypoattenuating to the muscle, and on MRI, tumors were iso- to minimally hypointense to muscle on T1-weighted images and hyperintense on T2-weighted images. Moderate, often heterogeneous, enhancement after

gadolinium injection was seen, and as expected, the larger tumors were heterogeneous on both CT and MRI, at times secondary to the presence of necrosis or hemorrhage. Central necrosis was seen in 25% of tumors, all of which belonged to the high-risk category (Table 1). Calcification and hemorrhage were seen in 12.5% cases each. This incidence of calcification is similar to the largest reported pathology series in which the incidence was 17%[15]. Mucosal involvement was identified on MRI in 25%, and was confirmed histologically in 3 cases. Although direct comparison of CT and MRI with respect to local staging was not systemically performed, we found that MRI, especially high-resolution T2-weighted images, particularly helpful in assessment of local tumor extent and prostatic invasion.

The tumors were moderately FDG avid, with a mean SUV_{max} of 11 (range 8.4−16.8, not very different from that previously reported for GISTs in other locations (mean SUV_{max} 5.8, range 1.4−19.7)[19]. Studies on GISTs in the stomach and small bowel suggest that FDG-PET has an incremental value over conventional imaging for the diagnostic and therapeutic management of patients with GISTs, however, there are limited data on the utility of FDG-PET/CT in the management of anorectal GISTs[20].

Metastatic disease at presentation was seen in 1 patient (6.3%), in the form of a solitary FDG-avid hepatic lesion. This lesion was also FDG avid, as expected. Although high incidence of hepatic metastases and intra-abdominal recurrence has been reported following surgery, metastases at the time of presentation has not been not reported in the previous series[8,15]. The lower incidence of metastatic disease at presentation may be related to extraperitoneal location of the tumors. Large studies comparing the incidence of metastasis with the more common sites, such as the stomach and small bowel, may be difficult given the rare nature of anorectal GISTs.

On pathology, most (93.7%) tumors were of spindle cell type with only 6.3% being mixed, predominantly epithelioid type. GISTs, originally classified as leiomyomas or leiomyosarcomas, are now readily distinguished from other mesenchymal gut tumors by the expression of KIT protein (CD117), a transmembrane receptor for stem cell factor[5]. By IHC, CD117 (KIT) positivity was present in all 16 anorectal GISTs (100%); all tested tumors expressed CD34 and were negative for desmin. SMA and S-100 markers were each positive in 22.2% of cases. These results were consistent with other large clinicopathologic series[15]. Although positivity for KIT (CD117) is constant in anorectal GISTs, the other antigens mentioned vary significantly and none of these are diagnostically specific for GISTs. The immunophenotype of true KIT-positive GISTs varies to some degree by location, with CD34 positivity seen most consistently in colorectal and esophageal lesions and SMA positivity seen most often in small intestinal GISTs[15].

Tumor size and mitotic index have been identified as important factors for risk stratification of primary GISTs (Table 1)[5]. In a previous study, most rectal GISTs >5 cm with any mitotic activity or those with >5 mitoses/50 HPF regardless of size showed aggressive behavior[15]. Anatomic site has also been suggested as an independent prognostic factor, with rectal, small bowel, and esophageal GISTs historically associated with worse prognosis than gastric primary tumors[5,21]. However, imatinib therapy, as neoadjuvant, adjuvant or primary treatment, has revolutionized the management of GISTs, and may influence the outcome of high-risk patients. Most of the tumors in our study (75%) belonged to the high-risk category.

The differential diagnosis of anorectal masses includes anorectal carcinoma, lymphoma and other mesenchymal tumors. Anorectal squamous cell carcinoma and adenocarcinoma tend to be circumferential tumors with luminal narrowing and infiltrative margins, show perirectal fat stranding, and frequently metastasize to lymph nodes, contrary to anorectal GISTs, which tend to be exophytic, non-circumferential, well-circumscribed tumors with expansile growth and without nodal metastases. Despite large tumor size, bowel obstruction is rarely seen with anorectal GISTs. Primary anorectal lymphoma mainly occurs in HIV-positive patients and often presents as an annular or eccentric mural mass with mucosal ulcerations. They tend to be homogeneous on imaging and can demonstrate intraluminal polypoid components, concentric wall thickening, fistula formation and adenopathy. Leiomyosarcomas at this site are exceedingly rare and tend to be large necrotic, hemorrhagic tumors without nodal metastases, similar in appearance to anorectal GISTs on imaging, and the diagnosis can usually be made only on histopathology. Malignant melanoma of the anorectum is a rare entity and only a few cases have been reported. Presence of high signal intensity on fat-saturated T1-weighted images, secondary to T1-shortening effects of melanin, may be helpful in the diagnosis.

Limitations of this study include its retrospective nature, and relatively small study population, given the rarity of this tumor. The imaging studies were not standardized; they were performed on different scanners using variable scanning protocols. MRI studies were performed using an endorectal coil or phased array body coils, with or without gadolinium contrast. The endorectal coil may limit the assessment of the intraluminal component of the tumor in some cases. Because our institution is a tertiary cancer center, the patients referred may not represent the true spectrum of disease in the general population. This may have influenced our radiologic findings including the paucity of high rectal tumors in our study, which may have been resected in the local institution with a simpler procedure without referral.

In conclusion, anorectal GISTs often present as well-circumscribed lobulated intramural or exophytic

FDG-avid hypoattenuating masses with a non-circumferential growth pattern that commonly extend into the ischiorectal fat without causing pelvic lymphadenopathy or bowel obstruction. Comparison with previously published data suggests that anorectal GISTs are similar in FDG avidity to GISTs at other locations. Prospective studies in a larger study population with standardized imaging protocols will enable better characterization of the imaging features of anorectal GISTs.

References

[1] DeMatteo RP, Lewis JJ, Leung D, Mudan SS, Woodruff JM, Brennan MF. Two hundred gastrointestinal stromal tumors: recurrence patterns and prognostic factors for survival. Ann Surg 2000; 231: 51–58. doi:10.1097/00000658-200001000-00008. PMid:10636102.

[2] Miettinen M, Sarlomo-Rikala M, Lasota J. Gastrointestinal stromal tumors: recent advances in understanding of their biology. Hum Pathol 1999; 30: 1213–1220. doi:10.1016/S0046-8177(99)90040-0. PMid:10534170.

[3] Kindblom LG, Remotti HE, Aldenborg F, Meis-Kindblom JM. Gastrointestinal pacemaker cell tumor (GIPACT): gastrointestinal stromal tumors show phenotypic characteristics of the interstitial cells of Cajal. Am J Pathol 1998; 152: 1259–1269. PMid:9588894.

[4] Corless CL, Fletcher JA, Heinrich MC. Biology of gastrointestinal stromal tumors. J Clin Oncol 2004; 22: 3813–3825. doi:10.1200/JCO.2004.05.140. PMid:15365079.

[5] Fletcher CDM, Berman JJ, Corless C, et al. Diagnosis of gastrointestinal stromal tumors: a consensus approach. Hum Pathol 2002; 33: 459–465. doi:10.1053/hupa.2002.123545. PMid:12094370.

[6] Demetri GD, von Mehren M, Blanke CD, et al. Efficacy and safety of imatinib mesylate in advanced gastrointestinal stromal tumors. N Engl J Med 2002; 347: 472–480. doi:10.1056/NEJMoa020461. PMid:12181401.

[7] Levy AD, Remotti HE, Thompson WM, Sobin LH, Miettinen M. Gastrointestinal stromal tumors: radiologic features with pathologic correlation. Radiographics 2003; 23: 283–304, 456; quiz 532.

[8] Levy AD, Remotti HE, Thompson WM, Sobin LH, Miettinen M. Anorectal gastrointestinal stromal tumors: CT and MR imaging features with clinical and pathologic correlation. AJR Am J Roentgenol 2003; 180: 1607–1612. PMid:12760929.

[9] van den Berg JC, van Heesewijk JP, van Es HW. Malignant stromal tumour of the rectum: findings at endorectal ultrasound and MRI. Br J Radiol 2000; 73: 1010–1012. PMid:11064658.

[10] Hama Y, Okizuka H, Odajima K, Hayakawa M, Kusano S. Gastrointestinal stromal tumor of the rectum. Eur Radiol 2001; 11: 216–219. doi:10.1007/s003300000615. PMid:11218017.

[11] Miettinen M, Sobin LH, Lasota J. Gastrointestinal stromal tumors of the stomach: a clinicopathologic, immunohistochemical, and molecular genetic study of 1765 cases with long-term follow-up. Am J Surg Pathol 2005; 29: 52–68. PMid:15613856.

[12] Miettinen M, Makhlouf H, Sobin LH, Lasota J. Gastrointestinal stromal tumors of the jejunum and ileum: a clinicopathologic, immunohistochemical, and molecular genetic study of 906 cases before imatinib with long-term follow-up. Am J Surg Pathol 2006; 30: 477–489. PMid:16625094.

[13] Miettinen M, Lasota J. Gastrointestinal stromal tumors: pathology and prognosis at different sites. Semin Diagn Pathol 2006; 23: 70–83. doi:10.1053/j.semdp.2006.09.001. PMid:17193820.

[14] Rumessen JJ, Vanderwinden J-M, Rasmussen H, Hansen A, Horn T. Ultrastructure of interstitial cells of Cajal in myenteric plexus of human colon. Cell Tissue Res 2009; 337: 197–212. doi:10.1007/s00441-009-0818-6. PMid:19506909.

[15] Miettinen M, Furlong M, Sarlomo-Rikala M, Burke A, Sobin LH, Lasota J. Gastrointestinal stromal tumors, intramural leiomyomas, and leiomyosarcomas in the rectum and anus: a clinicopathologic, immunohistochemical, and molecular genetic study of 144 cases. Am J Surg Pathol 2001; 25: 1121–1133. doi:10.1097/00000478-200109000-00002. PMid:11688571.

[16] Tworek JA, Goldblum JR, Weiss SW, Greenson JK, Appelman HD. Stromal tumors of the anorectum: a clinicopathologic study of 22 cases. Am J Surg Pathol 1999; 23: 946–54. doi:10.1097/00000478-199908000-00013. PMid:10435565.

[17] Hassan I, You YN, Dozois EJ, et al. Clinical, pathologic, and immunohistochemical characteristics of gastrointestinal stromal tumors of the colon and rectum: implications for surgical management and adjuvant therapies. Dis Colon Rectum 2006; 49: 609–615. doi:10.1007/s10350-006-0503-8. PMid:16552495.

[18] Shibata Y, Ueda T, Seki H, Yagihashi N. Gastrointestinal stromal tumour of the rectum. Eur J Gastroenterol Hepatol 2001; 13: 283–286. doi:10.1097/00042737-200103000-00012. PMid:11293450.

[19] Choi H, Charnsangavej C, Faria SC, et al. Correlation of computed tomography and positron emission tomography in patients with metastatic gastrointestinal stromal tumor treated at a single institution with imatinib mesylate: proposal of new computed tomography response criteria. J Clin Oncol 2007; 25: 1753–1759. doi:10.1200/JCO.2006.07.3049. PMid:17470865.

[20] Kaneta T, Takahashi S, Fukuda H, et al. Clinical significance of performing 18F-FDG PET on patients with gastrointestinal stromal tumors: a summary of a Japanese multicenter study. Ann Nucl Med 2009; 23: 459–464. doi:10.1007/s12149-009-0257-1. PMid:19430859.

[21] Emory TS, Sobin LH, Lukes L, Lee DH, O'Leary TJ. Prognosis of gastrointestinal smooth-muscle (stromal) tumors: dependence on anatomic site. Am J Surg Pathol 1999; 23: 82–87. doi:10.1097/00000478-199901000-00009. PMid:9888707.